Check for updates

Received: 16 July 2020 | Revised: 10 January 2021 | Accepted: 15 February 2021

DOI: 10.1002/mma.7358

SPECIAL ISSUE PAPER

WILEY

A graded mesh refinement approach for boundary layer originated singularly perturbed time-delayed parabolic convection diffusion problems

Kamalesh Kumar[1] | **Pramod Chakravarthy Podila**[1] | **Pratibhamoy Das**[2] | **Higinio Ramos**[3]

[1]Department of Mathematics, Visvesvaraya National Institute of Technology, Nagpur, India

[2]Department of Mathematics, Indian Institute of Technology, Patna, India

[3]Department of Applied Mathematics, Universidad de Salamanca, Salamanca, Spain

Correspondence
Pratibhamoy Das, Department of Mathematics, Indian Institute of Technology, Patna 801103, India.
Email: pratibhamoy@iitp.ac.in

Communicated by: D. Alexandrov

Funding information
Science and Engineering Research Board, Grant/Award Number: ECR/2017/001973

In this work, we consider a graded mesh refinement algorithm for solving time-delayed parabolic partial differential equations with a small diffusion parameter. The presence of this parameter leads to boundary layer phenomena. These problems are also known as singularly perturbed problems. For these problems, it is well-known that one cannot achieve a convergent solution to maintain the boundary layer dynamics, on a fixed number of uniform meshes irrespective of the arbitrary magnitude of perturbation parameter. Here, we consider an adaptive graded mesh generation algorithm, which is based on an entropy function in conjunction with the classical difference schemes, to resolve the layer behavior. The advantage of the present algorithm is that it does not require to have any information about the location of the layer. Several examples are presented to show the high performance of the proposed algorithm.

KEYWORDS

adaptive mesh algorithm, algorithmic complexity, boundary layer phenomena, entropy, graded mesh, parabolic convection–diffusion problems, time delay

MSC CLASSIFICATION

35K20; 35Q10; 34D15; 65Y20; 68Q25; 76M45

1 | INTRODUCTION

Boundary layer originated singularly perturbed parabolic PDEs (SPPPDEs) frequently appear in diverse areas, such as Mathematical Economics, Control theory, Biosciences, and Material Science.[1–4] As an example, one can look into the following time-delayed mathematical model of automatically controlled furnace to process metal sheets[5]:

$$\frac{\partial u_\varepsilon}{\partial t} = \varepsilon \frac{\partial^2 u_\varepsilon}{\partial x^2} + w(g(u_\varepsilon(x, t-\wp)))\frac{\partial u_\varepsilon}{\partial x} + d[f(u_\varepsilon(x, t-\tau)) - u_\varepsilon(x, t)].$$

Here, $u_\varepsilon(x, t)$ denotes the distribution of temperature in a metal sheet, which is moving with velocity w and heated by the temperature function f. Here, f and w are dynamically adapted by a controlling device which monitors the current temperature distribution. However, the finite speed of the controlling device introduces a fixed time lag/delay of length $\wp$. This type of problems is noted as differential-difference form due to the presence of time delay $\wp$. In this model, ε is an arbitrary small parameter which satisfies $0 < \varepsilon \ll 1$. The presence of this small diffusion parameter ε leads to the large

 © 2021 John Wiley & Sons, Ltd.

variation of the solution in a small region. This is called boundary/interior layer region. These problems are also known as singularly perturbed problems.

In early days, the approximation methods based on asymptotic analysis were a leading goal for several researchers for singularly perturbed problems. In the context of differential-difference equations, one of the motivational work on asymptotic analysis is by Lange and Miura.[6] Later, numerical methods using difference operators became popular as one can achieve an user chosen desired accuracy on an adaptive mesh.

It is well-known that the boundary/interior layer cannot be approximated by an uniform mesh on a fixed number of points unless a fitting is used[7] on the standard difference operator. This technique cannot be extended for several problems with parabolic boundary layers. This leads to the direction of layer adaptive mesh generation which is dense inside the boundary/interior layer regions. In recent years, a significant research on adaptive mesh generation has been observed for numerical study of these models.

Few of the researches in the context of adaptive mesh include previous studies.[8–10] Note that the presence of a delay term can change the nature of the solution. For example, a time-delayed system[11] can have multiple layer phenomena in singular perturbation context. Hence, the numerical analysis of large time-delayed SPPPDEs became the center of interest by several researchers; see, for example, Ansari and Shishkin[12] on piecewise uniform meshes and Gowrisankar and Natesan[13] on adaptive meshes. There are other ways to find an approximation of the solution based on perturbation theory, which can be seen in previous studies.[14–17] It turns out that the smoothness of the initial data and the structure of the a priori meshes play important roles on the error estimates and convergence of the numerical solutions for SPPs; see, for example, Das and Natesan,[18] Chandru et al.[19,20] and Govindarao et al.[21] Uniformly convergent numerical methods for the SPPs with delay and advance terms can be also observed in Bansal et al.[22,23] on a priori fixed meshes. This mesh structure has been also adaptively improved by Chakravarthy and Kumar[24] by a new strategy.

In general, the low order upwind schemes are mainly popular for singularly perturbed problems. Based on the upwind schemes, several uniformly convergent numerical methods are developed on equidistributed meshes where the number of mesh points is not dependent on perturbation parameter. On equidistributed meshes, one can achieve the optimal convergent solution by using upwind schemes for convection–diffusion problems, which is not possible on Shishkin meshes. Very recently, the researches developed in other works[25–30] have used the equidistributed meshes to obtain optimal convergent solutions on a fixed number mesh points. Note that one can achieve lower order accurate solution in case first-order upwind schemes are used for convection term.

The rate of accuracy of the lower order upwind schemes can be also greatly improved by postprocessing methods, like Richardson extrapolation technique.[18] However, it is tempting to approximate the continuous SPPPDEs by using the well-known central difference approximation, as this approximation leads to less consistency error compared to first-order upwind schemes. But this discretization leads to an oscillatory solution, which does not reflect the physical structure of the analytical solution. To handle such situation, we need a larger number of mesh points at the regions where the solution becomes oscillatory. Depending on the model problems, several priori meshes like, Bakhvalov,[31] Gartland,[32] and Beckett[33,34] are developed to overcome this drawback. Nevertheless, all of the above meshes require a priori information about the location and the width of the layer.

In the present research, our aim is to generate a new graded mesh which will automatically introduce new mesh points to the region of large variation. The new algorithm has two purposes. We wanted to have higher-order accurate solutions, say by using central difference schemes. Then, we want to remove the nonphysical oscillations, appearing in higher-order numerical schemes, by introducing more points in the region of oscillations. To do this, we have used the entropy of the numerical solutions. In addition to this graded mesh generating algorithm,[35] this research shows the effectiveness of this algorithm to solve the time-delayed SPPPDEs. This algorithm is adaptive and does not require any a priori knowledge about the layer location.

Organization of the paper: In Section 2, we consider the time-delayed SPPPDE which will be used for present analysis. In addition, we also provide few compatibility conditions on the data which can be extended for required smoothness of the solution. In Section 3, we discretize the problem and consider an algorithm for generating layer adaptive mesh. To show the effectiveness of the present approach, we have considered three problems for numerical experiments in Section 5. Concluding remarks are given in the final section.

2 | PROBLEM STATMENT

In this work, we consider the following class of time-delayed SPPPDEs:

$$L_\varepsilon u(x,t) \equiv \frac{\partial u}{\partial t} - \varepsilon \frac{\partial^2 u}{\partial x^2} + p(x,t)\frac{\partial u}{\partial x} + q(x,t)u(x,t) = -r(x,t)u(x,t-\wp) + g(x,t),\ (x,t) \in \Omega, \tag{1}$$

with the initial condition

$$u(x,t) = \Psi_m(x,t),\ \ (x,t) \in \Upsilon_m,$$

and boundary conditions

$$u(0,t) = \Psi_l(t),\ \text{on } \Upsilon_l,\ \text{and } u(1,t) = \Psi_r(t),\ \text{on } \Upsilon_r. \tag{2}$$

Here, $(0 < \varepsilon \ll 1)$ is the perturbation parameter, $\wp$ is the time delay, $\Omega = \mathbb{S}\times(0,\mathbb{T}]$ where $\mathbb{S} = (0,1)$. Let $\Upsilon = \Upsilon_l \cup \Upsilon_m \cup \Upsilon_r$, where $\Upsilon_m = \overline{\mathbb{S}} \times [-\wp, 0]$ for $0 < \wp < \mathbb{T}$ and $\Upsilon_l = \{(0,t) : 0 \le t \le \mathbb{T}\}$, $\Upsilon_r = \{(1,t) : 0 \le t \le \mathbb{T}\}$ be, respectively, the left and the right boundaries of the domain $\bar{\Omega}$. Here, $\bar{\Omega}$ defines the closure of the set Ω.

The functions $p(x,t)$, $q(x,t)$, $r(x,t)$, $g(x,t)$, $\Psi_m(x,t)$, $\Psi_l(t)$, and $\Psi_r(t)$ are considered to be sufficiently smooth functions, which satisfy

$$p(x,t) \ge \alpha > 0,\ q(x,t) \ge 0,\ r(x,t) \ge \beta > 0\ \text{ on }\ \bar{\Omega},$$

for some real positive values α and β. Under the above conditions, the solution of the problems (1) and (2) exhibits regular boundary layer near $x = 1$ of width $\mathcal{O}(\varepsilon)$.[19,22]

Now, we assume that all the given data satisfy certain compatibility conditions, and the given functions are Hölder continuous.[36] The zeroth and first-order compatibility conditions are

$$\Psi_m(0,0) = \Psi_l(0),$$

$$\Psi_m(1,0) = \Psi_r(0), \tag{3}$$

$$\frac{d\Psi_l(0)}{dt} - \varepsilon\frac{\partial^2 \Psi_m(0,0)}{\partial x^2} + p(0,0)\frac{\partial \Psi_m(0,0)}{\partial x} + q(0,0)\Psi_m(0,0) = -r(0,0)\Psi_m(0,-\wp) + g(0,0)$$

and

$$\frac{d\Psi_r(0)}{dt} - \varepsilon\frac{\partial^2 \Psi_m(1,0)}{\partial x^2} + p(1,0)\frac{\partial \Psi_m(1,0)}{\partial x} + q(1,0)\Psi_m(1,0) = -r(1,0)\Psi_m(1,-\wp) + g(1,0). \tag{4}$$

The existence and uniqueness of the solution of (1) can be observed from Solonnikov et al.[36] based on the above conditions. The time-delayed singularly perturbed problem (1) satisfies the following minimum principle.

Lemma 1 (Minimum principle[13,18,19]). *Let the function $\varphi(x,t) \in C^2(\Omega) \cap C^0(\bar{\Omega})$, such that $\varphi(x,t) \ge 0$ on Υ and $L_\varepsilon \varphi(x,t) \ge 0$ on Ω where L_ε is defined in (1). Then $\varphi(x,t) \ge 0$ on $\bar{\Omega}$.*

In addition, the solution and its first derivative satisfy the following bounds.

Theorem 1. *For $n = 0, 1$, the solution $u(x,t)$ of (1) and (2) and its first derivative satisfy*

$$\left|\frac{\partial^n u(x,t)}{\partial x^n}\right| \le C\left(1 + \varepsilon^{-n}\exp(-\alpha(1-x)/\varepsilon)\right),\ \ on\ \ \Omega,$$

where C is a generic positive constant which is independent of ε.

Proof. The above result can be obtained from Bansal et al.[22] □

The above a priori bound shows that the solution of (1) and (2) is uniformly bounded. We note that the bound for its first derivative depends on the inverse power of ε at Ω.

3 | DISCRETE PROBLEM AND ADAPTIVE STRATEGY

To develop a space-time numerical approximation for solving the time-delayed SPPPDE (1) with the initial and boundary conditions (2), we will consider a combination of two different schemes: a uniform discretization in time and an adapted discretization in space. The time domain $[0, \mathbb{T}]$ is divided into M_t parts with fixed mesh size Δt. The mesh size Δt is chosen in the way such that the delay term satisfies $\wp = s\Delta t$, for some positive integer s. In addition, we choose $\mathbb{T} = M_t \Delta t$ for some positive integer M_t. Therefore, $\{0 = t_0 < t_1 < \ldots < t_{M_t} = \mathbb{T}\}$ will be the mesh points in time, where $t_j = j\frac{\mathbb{T}}{M_t} = j\Delta t$, $j = 0, 1, \ldots, M_t$.

For the time discretization, we use the stable backward Euler's scheme and convert the problem (1) into semi discretization form, as follows:

$$\frac{U^j(x) - U^{j-1}(x)}{\Delta t} - \varepsilon \frac{d^2U^j(x)}{dx^2} + p^j(x)\frac{dU^j(x)}{dx} + q^j(x)U^j(x) = -r^j(x)U^{j-s}(x) + g^j(x), \tag{5}$$

where $U^j(x) = U(x, t_j)$ is an approximation of $u(x, t_j)$, $q^j(x) = q(x, t_j)$, $r^j(x) = r(x, t_j)$, and $g^j(x) = g(x, t_j)$, for $j = 1, 2, \ldots, M_t$.

At each time step, Equation (5) takes the following form:

$$-\varepsilon \frac{d^2U^j(x)}{dx^2} + p^j(x)\frac{dU^j(x)}{dx} + P^j(x)U^j(x) = Q^j(x), \quad \text{for } j = 1, 2, \ldots, M_t, \tag{6}$$

where $P^j(x) = P(x, t_j) = q^j(x) + 1/\Delta t$ and $Q^j(x) = Q(x, t_j) = g^j(x) + U^{j-1}(x)/\Delta t - r^j(x)U^{j-s}(x)$.

The corresponding given conditions are

$$\begin{gathered} U^j(x) = \Psi_m(x, t_j), \quad x \in [0, 1], \quad j = -s, -s+1, \ldots, 0, \\ U^j(0) = \Psi_l(t_j), \quad j = 1, 2, \ldots, M_t, \\ U^j(1) = \Psi_r(t_j), \quad j = 1, 2, \ldots, M_t. \end{gathered} \tag{7}$$

By using the initial data, we can rewrite $Q^j(x)$ as

$$Q^j(x) = \begin{cases} g^j(x) + \frac{U^{j-1}(x)}{\Delta t} - r^j(x)\Psi_m^{j-s}(x) & \text{for } j = 0, 1, 2, \ldots, s, \\ g^j(x) + \frac{U^{j-1}(x)}{\Delta t} - r^j(x)U^{j-s}(x) & \text{for } j = s+1, s+2, \ldots, M_t, \end{cases}$$

where $\Psi_m^{j-s}(x) = \Psi_m(x, t_{j-s})$.

Lemma 2. *The error estimates associated with (6), that is, $e_j = u(x, t_j) - U^j(x)$, satisfy the following estimates:*

$$||e_j|| \leq C\Delta t.$$

Proof. The proof can be easily done by calculating the TE in (6) and after that taking the summation of all local error for each time level. The result can be noted from Das and Mehrmann.[37] □

3.1 | Difference operators

We use the following difference operators in space for discretizing $U^j(x)$ on a general nonuniform mesh $\{0 = x_0 < x_1 < \ldots < x_{M_x} = 1\}$ in space with $M_x + 1$ points:

$$D_x^+ U_i^j = \frac{U_{i+1}^j - U_i^j}{x_{i+1} - x_i}, \; D_x^- U_i^j = \frac{U_i^j - U_{i-1}^j}{x_i - x_{i-1}}, \; D_x^0 U_i^j = \frac{U_{i+1}^j - U_{i-1}^j}{x_{i+1} - x_{i-1}},$$

where D_x^+, D_x^-, and D_x^0 are the forward, backward, and central difference operators, respectively.

For the discretization of second-order derivative, the standard central difference operator in space is defined as

$$D_x^2 U_i^j = \frac{2(D_x^+ U_i^j - D_x^- U_i^j)}{x_{i+1} - x_{i-1}}.$$

Let $h_i = x_{i+1} - x_i$ denote the step sizes of the spatial nonuniform mesh.

Now, we discretize (6) on the nonuniform mesh with the help of the above operators. We define the discrete problem as follows:

$$-\varepsilon \frac{2(D_x^+ U_i^j - D_x^- U_i^j)}{h_i + h_{i-1}} + p^j(x_i) \frac{U_{i+1}^j - U_{i-1}^j}{h_i + h_{i-1}} + P^j(x_i) U_i^j = Q(x_i, t_j), \tag{8}$$

where

$$Q_i^j = \begin{cases} g^j(x_i) + \frac{U_i^{j-1}}{\Delta t} - r^j(x_i)\Psi_m^{j-s}(x_i) & \text{for } j = 0, 1, 2, \ldots, s, \\ g^j(x_i) + \frac{U_i^{j-1}}{\Delta t} - r^j(x_i) U_i^{j-s} & \text{for } j = s+1, s+2, \ldots, M_t. \end{cases}$$

Equation (8) can be written in the form:

$$S_{i,j}^- U_{i-1}^j + S_{i,j}^c U_i^j + S_{i,j}^+ U_{i+1}^j = Q_i^j, \tag{9}$$

for $i = 1, \ldots, M_x$ and $j = 1, \ldots, M_t$, where

$$\begin{aligned} S_{i,j}^- &= \frac{-2\varepsilon}{h_{i-1}(h_i + h_{i-1})} - \frac{p^j(x_i)}{h_i + h_{i-1}}, \\ S_{i,j}^c &= \frac{2\varepsilon}{h_i(h_i + h_{i-1})} + \frac{2\varepsilon}{h_{i-1}(h_i + h_{i-1})} + q^j(x_i) + \frac{1}{\Delta t}, \\ S_{i,j}^+ &= \frac{-2\varepsilon}{h_i(h_i + h_{i-1})} + \frac{p^j(x_i)}{h_i + h_{i-1}}. \end{aligned} \tag{10}$$

Initially, we solve the system (9) with the boundary conditions (7) with a fixed number of uniformly distributed mesh points in spatial direction. Nevertheless, due to the presence of ε, there will be oscillations in the surface. To remove these oscillations, more number of mesh points would be required in the layer zone, if one restricts to uniform meshes for an arbitrary small ε. We generate an adaptive spatial mesh using the entropy functions property, which will introduce more number of mesh points in the oscillatory region, in order to avoid the oscillations of the numerical solution on a uniform mesh. The algorithm for generating this mesh is presented in Section 3.2.

Now, let us assume that M_x^* is the number of mesh points which are required to get an adaptive mesh on which a nonoscillatory solution can be obtained. Let us define the step sizes as $h_i = x_{i+1} - x_i$, for $i = 1, \ldots, M_x^*$. From (10), we get

$$S_{i,j}^c + S_{i,j}^- + S_{i,j}^+ = q^j(x_i) + \frac{1}{\Delta t} > 0,$$

since $q^j(x_i) \geq 0$ on Ω and Δt is the temporal step size. This shows that the system (9) is diagonally dominant. Note also that $S_{i,j}^+ < 0$, for $h_i p^j(x_i) < 2\varepsilon$, that is, for some $O(h_i, h_{i-1}) < \varepsilon$. Again $S_{i,j}^- < 0$.

Note that the mesh adaptation strategy requires dense points inside the boundary layer region. Outside the boundary layer, the step sizes are supposed to be coarser than in the layer region. It can be seen in Andreev and Kopteva[38] that the central difference scheme in (8) leads to a nonoscillatory solution, if $h_i/2 \leq \varepsilon$ for $p(x) = 1$. For a self-adjoint problem $-u''(x) - (b(x)u(x))' = g(x)$, the required condition for nonoscillatory solution based on central difference scheme is $h_i b_{i-1}/2 \leq \varepsilon$. They have also provided an almost second-order convergence on a nonuniform mesh.

3.2 | Mesh selection strategy

Let us consider (6)

$$-\varepsilon \frac{d^2 U^j(x)}{dx^2} + p^j(x) \frac{dU^j(x)}{dx} + P^j(x) U^j(x) = Q^j(x).$$

From the theory of scalar conservation law and the viscosity solution, it is well-known that $U^j(x)^2$ can be chosen as a perfect entropy variable; see, for example, Kumar and Srinivasan and Leveque.[35,39] To define the entropy production equation, we multiply the above equation by $2U^j(x)$ and obtain

$$\left(-\varepsilon\frac{d^2U^j(x)}{dx^2}+p^j(x)\frac{dU^j(x)}{dx}+P^j(x)U^j(x)\right)*2U^j(x)=Q^j(x)*2U^j(x). \tag{11}$$

After some simplifications, (11) can be written as

$$-\varepsilon\frac{d^2Z^j(x)}{dx^2}+p^j(x)\frac{dZ^j(x)}{dx}+2P^j(x)Z^j(x)+2\varepsilon\left(\frac{dU^j(x)}{dx}\right)^2=2U^j(x)Q^j(x),$$

where $Z^j(x)=(U^j(x))^2$.

Now, we rearrange the above differential equation as follows:

$$-\varepsilon\frac{d^2Z^j(x)}{dx^2}+p^j(x)\frac{dZ^j(x)}{dx}-2U^j(x)Q^j(x)=-2P^j(x)Z^j(x)-2\varepsilon\left(\frac{dU^j(x)}{dx}\right)^2. \tag{12}$$

Let us define the entropy function E^j as

$$E^j(x)=-2P^j(x)Z^j(x)-2\varepsilon\left(\frac{dU^j(x)}{dx}\right)^2.$$

Note that $P^j(x)>0$, $Z^j=(U^j)^2\geq 0$ and $(dU^j/dx)^2\geq 0$ for all $x\in\mathbb{S}=(0,1)$. Therefore, $E^j(x)$ is always negative for $x\in\mathbb{S}=(0,1)$ at every time level. Now, we discretize $E^j(x)$ at the mesh point (x_i,t_j), using the forward and backward difference operators in Section 3.1, as

$$E_i^j=\left[-2P_i^j(U_{i+1}^jU_{i-1}^j)\right]+\left[-2\varepsilon\left(\frac{U_i^j-U_{i-1}^j}{x_i-x_{i-1}}\right)\left(\frac{U_{i+1}^j-U_i^j}{x_{i+1}-x_i}\right)\right]. \tag{13}$$

We know that the central difference approximations for Equation (6) lead to nonphysical oscillations in the solution. Hence, if one calculates E_i^j using this oscillatory solution, it can be observed that E_i^j will become negative where the solution is smooth (i.e., outside the boundary layers) as the second term in the right-hand side of (13) will be of order $O(\varepsilon)$, and hence, it will be comparatively smaller than the first term for $0<\varepsilon\ll 1$ (see Theorem 1). This is matched with the analytical behavior of $E^j(x)$. But, the discrete approximation E_i^j will become positive inside the boundary layer region, as here, the second term will be dominant than the first term since the solution derivative is of $O(\varepsilon^{-1})$ for $0<\varepsilon\ll 1$, and $(U_i^j-U_{i-1}^j)(U_{i+1}^j-U_i^j)<0$. This does not match with the analytical behavior of $E^j(x)$. Hence, our job is to devise an algorithm which will introduce more mesh points at these regions. We search for the mesh points where the highest oscillation occurs with the help of the entropy function and introduce new mesh points on the left and on the right sides of it. The oscillatory behavior of the numerical solution in a neighborhood of the point x_i is shown in Figures 1 and 2 for the two possible cases. These figures are important to understand the location of introducing new mesh points.

Since the boundary layer location and its width do not vary with respect to time, it would be beneficial to adapt the space mesh only at time stage $t=\Delta t$ with entropy function E^1 and fix this adaptive mesh over all time level. The following algorithm introduces new mesh points in the spatial direction whenever the oscillation is maximum, in order to get an oscillation-free numerical solution.

3.3 | Graded mesh refinement algorithm

Step 1. Choose an initial uniform mesh in space with M_x+1 points in the spatial direction. Let us divide the time domain with M_t uniform partitions with step size Δt. At $t_1=\Delta t$, let us call this space-time mesh at (X_{M_x},t_1). Go to **Step 2**.

Step 2. Compute the numerical solution on (X_{M_x},t_1) using (9) and go to **Step 3**.

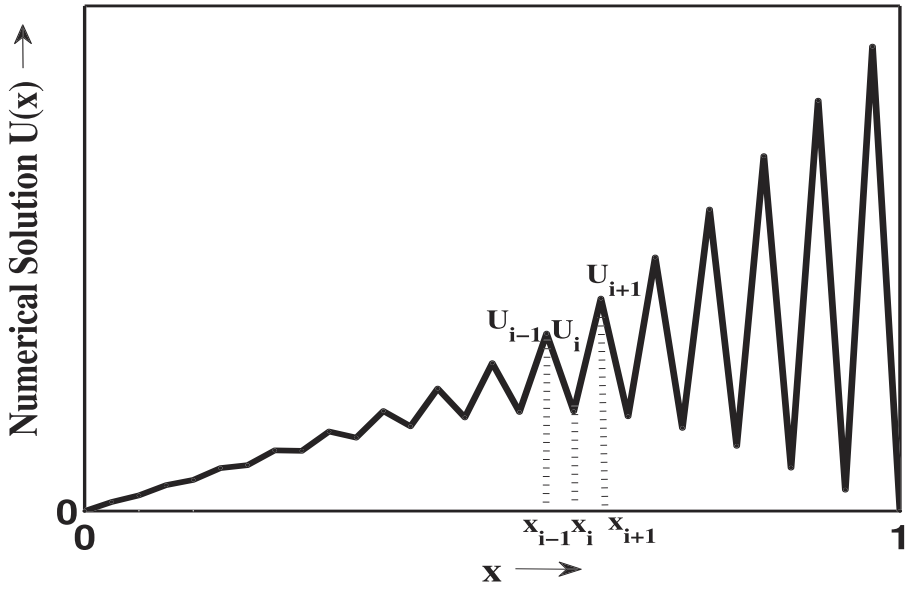

FIGURE 1 Oscillation in numerical solution at the point x_i, when $U_i - U_{i-1} < 0$ and $U_{i+1} - U_i > 0$

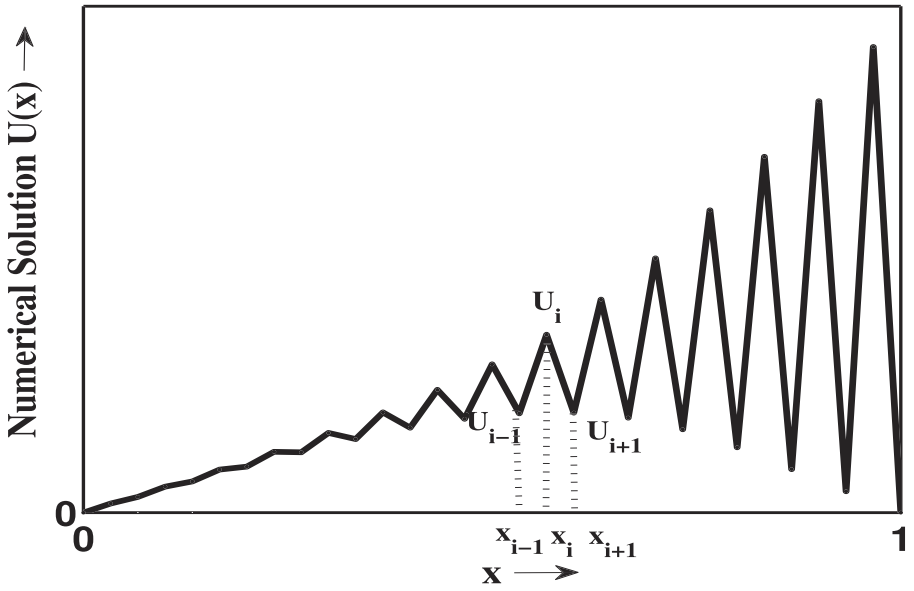

FIGURE 2 Oscillation in numerical solution at point x_i, when $U_i - U_{i-1} > 0$ and $U_{i+1} - U_i < 0$

Step 3. Calculate the entropy E_i^1 on each point $(x_i, t_1)_{i=2:M_x}$ at time t_1 using (13) and fix $E_1^j = E_{M_x+1}^j = 0$ at the boundary points over all time level $t = t_j$.

if $\max_i(E_i^1) > 0$ and $\max_i(E_i^1) = E^1|_{x=x_k}$ **then**

Add one mesh point on the left and another one on the right side of the mesh point x_k to generate a set of new nonuniform mesh points. Let $M_x^* = M_x + 2$. Now, go to **Step 2** to repeat the process with $M_x^* + 1$ space mesh points, and $M_x = M_x^*$.

else if $\max_i(E_i^1) \leq 0$ **then**

No new mesh point is required. Stop the iterative process. $(X_{M_x^*}, t_1)$ is the final adaptive mesh at $t = t_1$, which will be fixed at all time level. **end if**

4 | ERROR ANALYSIS

In this section, we have presented the error analysis of the scheme. The scheme in (9) can be written as

$$Au^j = B,$$

where matrix A is a tridiagonal matrix, $u^j = (u_1^j, u_2^j, \dots, u_{M_x+1}^j)^t$, and $B = Q_i^j$. From (9), we have,

$$|S_{i,j}^c| > |S_{i,j}^- + S_{i,j}^+|,$$

which shows that the matrix A is diagonally dominant. The scheme is stable, and u_i^j can be obtained at each time level.

Next, we calculate the T.E. of the scheme. Considering $u_i^j = u(x_i, t_j)$, from Taylor's series expansion, we have

$$u_{i+1}^j = u_i^j + h_i(u_x)_i^j + \frac{h_i^2}{2!}(u_{xx})_i^j + \frac{h_i^3}{3!}(u_{xxx})_i^j + \dots, \tag{14}$$

$$u_{i-1}^j = u_i^j - h_{i-1}(u_x)_i^j + \frac{h_{i-1}^2}{2!}(u_{xx})_i^j - \frac{h_{i-1}^3}{3!}(u_{xxx})_i^j + \dots, \tag{15}$$

and

$$u_i^{j-1} = u_i^j + \Delta t(u_t)_i^j + \frac{\Delta t^2}{2!}(u_{tt})_i^j + \frac{\Delta t^3}{3!}(u_{ttt})_i^j + \dots. \tag{16}$$

Here, we find the TE in the different time intervals. First, we calculate the error on the interval $[0, \wp]$. On the first partition $[0, \wp]$, note that the right-hand side of (1) at jth time level is depending on the solution at $(j-1)$th time level. Here, $\wp$ is independent of ε.

Using the Taylor's series in (9), and neglecting higher-order terms, we have truncation error (T.E.)

$$\begin{aligned}
T.E. &= S_{i,j}^- \left(u_i^j - h_{i-1}(u_x)_i^j + \frac{h_{i-1}^2}{2!}(u_{xx})_i^j - \frac{h_{i-1}^3}{3!}(u_{xxx})_i^j \right) + S_{i,j}^c u_i^j + S_{i,j}^+ \left(u_i^j + h_i(u_x)_i^j + \frac{h_i^2}{2!}(u_{xx})_i^j + \frac{h_i^3}{3!}(u_{xxx})_i^j \right) \\
&\quad - g^j(x_i) - \Delta t \left(u_i^j - \Delta t(u_t)_i^j + \frac{\Delta t^2}{2!}(u_{tt})_i^j + \frac{\Delta t^3}{3!}(u_{ttt})_i^j \right) + r^j(x_i)\Psi_m^{j-s}(x_i), \\
&= (S_{i,j}^- + S_{i,j}^c + S_{i,j}^+)u_i^j + (-h_{i-1}S_{i,j}^- + h_i S_{i,j}^+)(u_x)_i^j + \left(\frac{h_{i-1}^2}{2!}S_{i,j}^- + \frac{h_i^2}{2!}S_{i,j}^+ \right)(u_{xx})_i^j + \left(-\frac{h_{i-1}^3}{3!}S_{i,j}^- + \frac{h_i^3}{3!}S_{i,j}^+ \right)(u_{xxx})_i^j \\
&\quad - g^j(x_i) - \Delta t \left(u_i^j - \Delta t(u_t)_i^j + \frac{\Delta t^2}{2!}(u_{tt})_i^j + \frac{\Delta t^3}{3!}(u_{ttt})_i^j \right) + r^j(x_i)\Psi_m^{j-s}(x_i), \\
T.E. &= \frac{p^j(x_i)(h_i - h_{i-1})}{2}(u_{xx})_i^j - \frac{\Delta t}{2}(u_{tt})_i^j + \left(\frac{-\varepsilon(h_i - h_{i-1})}{3} + \frac{p^j(x_i)(h_{i-1}^3 + h_i^3)}{h_{i-1} + h_i} \right)(u_{xxx})_i^j + \frac{\Delta t^2}{6}(u_{ttt})_i^j.
\end{aligned}$$

As $h_i, h_{i-1} \to 0$ and $\Delta t \to 0$, the TE is going to zero, which shows that the scheme is consistent and TE of the scheme is of order $O(h_i - h_{i-1}, \Delta t)$ on the interval $[0, \wp]$. Similarly, one can find the TE on the intervals $[\wp, 2\wp], [2\wp, 3\wp], [3\wp, 4\wp], \dots, [(n-1)\wp, n\wp]$ for all $n \le \mathbb{T}/\wp$.

Hence, from the Lax Equivalence theorem, the finite difference approximation, which is consistent and stable, is necessary and sufficient for convergence to the exact solution of a well-posed PDE.

5 | NUMERICAL EXPERIMENTS

Now, we show the effectivity of the present algorithm for parabolic problems with time delay by taking few test problems. We start with a user-chosen uniform mesh and use the entropy function to locate the position where the new mesh points need to be introduced by Algorithm 3.3. The adaptive mesh has been generated at the time level $t = \Delta t$, and it is kept fixed over all time levels as the boundary layer will not vary in time. For a given number of partitions M_x, let us assume that a total $M_x^* + 1$ number of space mesh points are required for an oscillatory-free solution. We find out the numerical errors on these mesh points for a given M_x, ε and $\wp$.

The maximum absolute pointwise errors are presented for different values of the perturbation parameters, whenever the exact solution is available. These errors are defined as follows[19]:

$$E_\varepsilon^{M_x^*, M_t} = \max_{0 \le i \le M_x^*, 0 \le j \le M_t} |U^{M_x^*, M_t}(x_i, t_j) - u(x_i, t_j)|.$$

If the exact solution is unknown, we use the following double mesh technique[40] to calculate the maximum absolute errors:

$$E_{\epsilon}^{M_x^*,M_t} = \max_{0\le i\le M_x^*, 0\le j\le M_t} |U^{M_x^*,M_t}(x_i,t_j) - U^{2M_x^*,2M_t}(x_{2i},t_{2j})|.$$

Based on this principle, we bisect the final adaptive mesh in space direction as well as in time direction to get $U^{2M_x^*,2M_t}$.

Example 1. First, we consider the following time-delayed SPPPDE[13] for adaptive mesh generation

$$u_t - \varepsilon u_{xx} + (1 + x - x^2)u_x - u(x,t-1) = g(x,t),\ (x,t) \in (0,1)\times(0,2],$$

with the initial data

$$u(x,t) = \Psi(x,t),\quad (x,t) \in [0,1]\times[-1,0],$$

and the boundary conditions

$$u(0,t) = 0,\ and\ u(1,t) = 0,\quad t \in (0,2].$$

To produce the errors, we assume the exact solution of this problem as

$$u(x,t) = \exp(-t)(a_1 + xa_2 - \exp((x-1)/\varepsilon)),$$

which contains the boundary layer function. Here, $a_1 = \exp(-1/\varepsilon)$ and $a_2 = 1 - \exp(-1/\varepsilon)$. Here, $g(x,t)$ and $\Psi(x,t)$ are chosen so that the above function becomes the exact solution of this example. The numerical solutions based on the uniform mesh and the numerical solutions based on the proposed adaptive mesh obtained by present Algorithm 3.3 are plotted in Figures 3 and 4, respectively, for Example 1 respectively at different time levels. Solution surface plots for Example 1 with $\varepsilon = 2^{-10}$ and $\wp = 1$, on these two meshes, are also provided in Figures 5 and 6. One can observe the oscillatory behavior of the numerical solution based on central difference scheme on uniform mesh at Figures 3 and 5. From these figures, it can be pointed out that the unstable oscillatory behavior of the numerical solution can be removed by using the proposed approach.

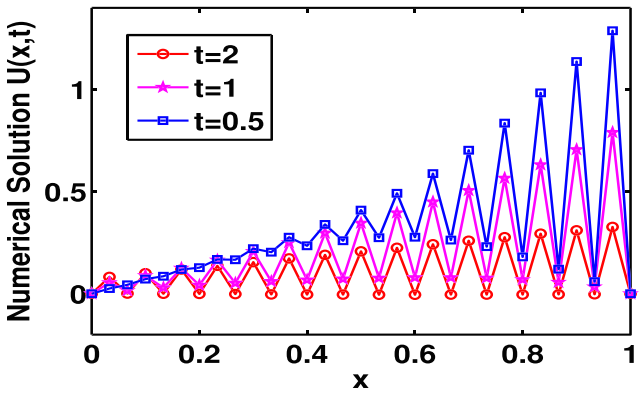

FIGURE 3 Oscillatory non physical numerical solutions of Example 1 with $\varepsilon = 2^{-10}$, $M_x = 20$, and $M_t = 20$ on uniform mesh at different time levels [Colour figure can be viewed at wileyonlinelibrary.com]

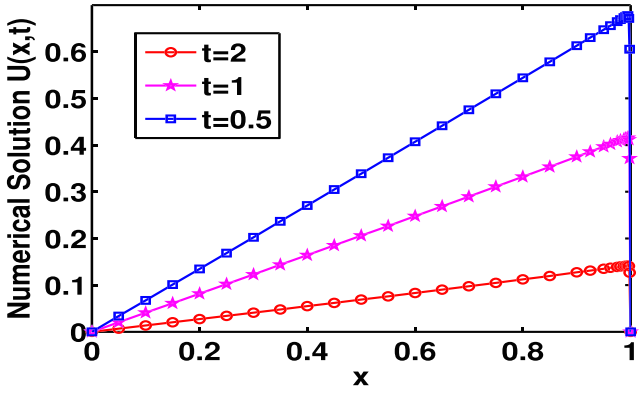

FIGURE 4 Nonoscillatory numerical solutions of Example 1 with $\varepsilon = 2^{-10}$, $M_x = 20$, $M_x^* = 30$, and $M_t = 20$ on adaptive mesh at different time levels [Colour figure can be viewed at wileyonlinelibrary.com]

The adaptive mesh structure, obtained by the Algorithm 3.3 for $\varepsilon = 2^{-10}$ with 11 and 21 numbers of initial uniform mesh points, is presented at Figures 7 and 8, respectively. To show the efficiency of the present algorithm, we also present the maximum pointwise errors in Table 1 for different values of the perturbation parameter ε.

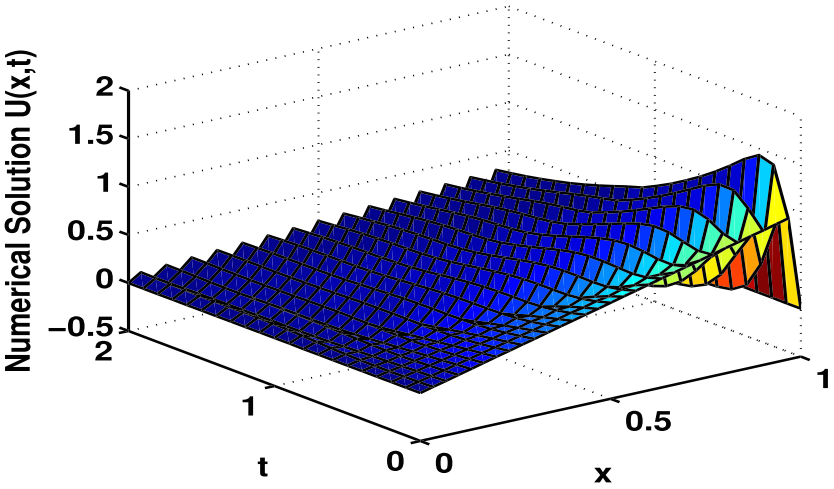

FIGURE 5 Oscillatory solution surface plot of Example 1, using uniform mesh, for $\varepsilon = 2^{-10}$, $M_x = 20$, and $M_t = 20$ [Colour figure can be viewed at wileyonlinelibrary.com]

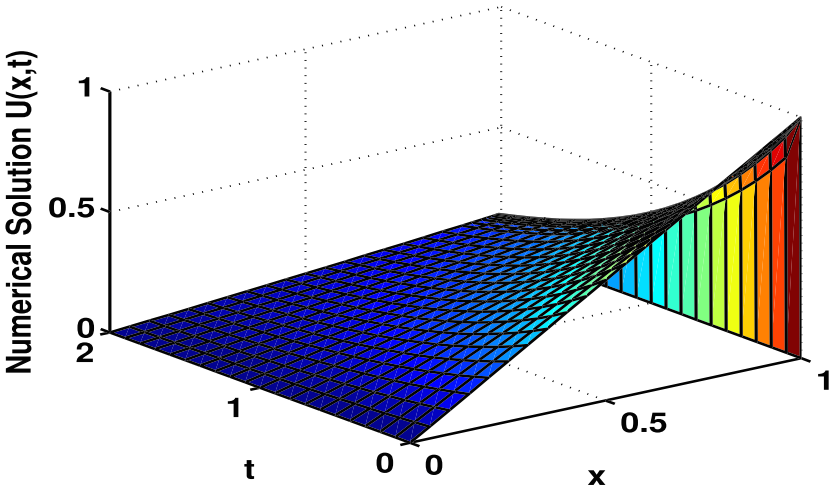

FIGURE 6 Nonoscillatory solution surface plot of Example 1 on the adaptive mesh, for $\varepsilon = 2^{-10}$, $M_x = 20$, $M_x^* = 30$, and $M_t = 20$ [Colour figure can be viewed at wileyonlinelibrary.com]

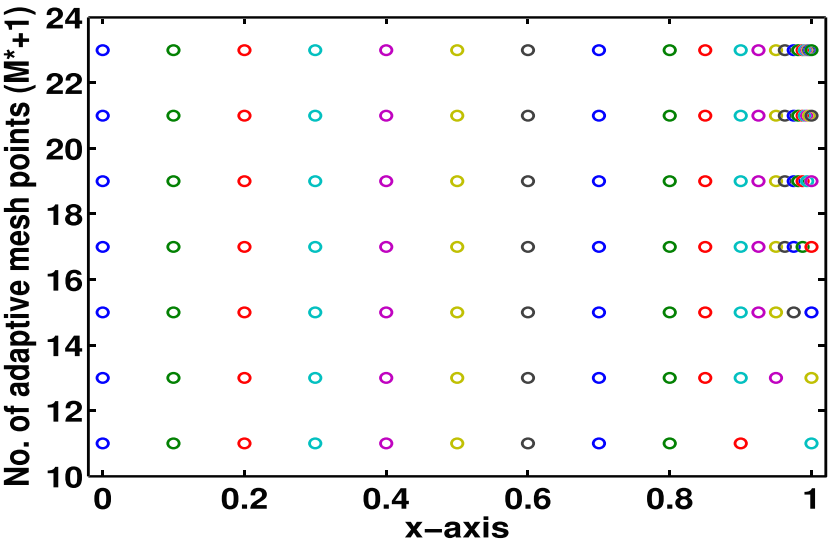

FIGURE 7 Generation of adaptive meshes from uniform meshes (starting with $M_x = 10$), for $\varepsilon = 2^{-10}$ at $t = 1/10$ for Example 1 [Colour figure can be viewed at wileyonlinelibrary.com]

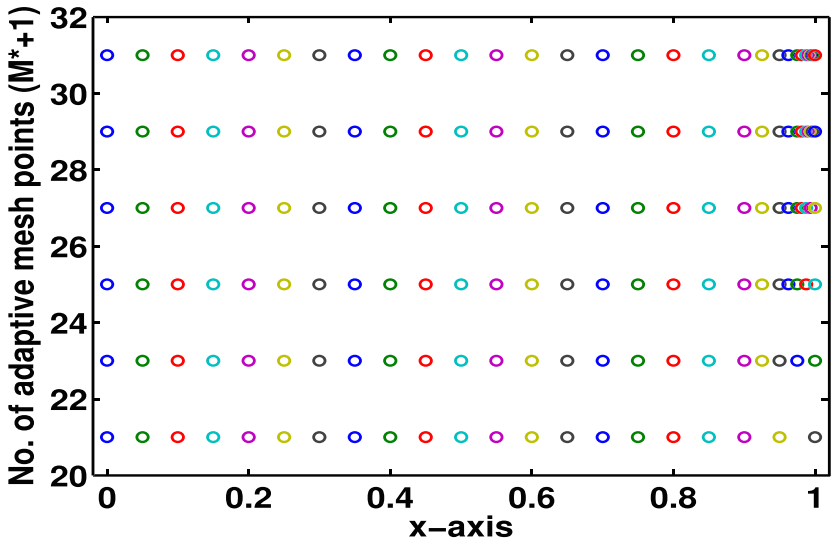

FIGURE 8 Generation of adaptive meshes from uniform meshes (starting with $M_x = 20$), for $\varepsilon = 2^{-10}$ at $t = 1/10$ for Example 1 [Colour figure can be viewed at wileyonlinelibrary.com]

ε	M_x^*	$E_\varepsilon^{M_x^*,M_t}$
2^{-10}	30	8.8166e-02
2^{-11}	32	8.7022e-02
2^{-12}	34	8.6442e-02
2^{-13}	36	8.6149e-02
2^{-14}	38	8.6002e-02
2^{-15}	40	8.5928e-02
2^{-16}	42	8.5891e-02
2^{-17}	44	8.5873e-02
2^{-18}	46	8.5864e-02
2^{-19}	48	8.5859e-02
2^{-20}	50	8.5857e-02
2^{-21}	52	8.5856e-02
2^{-22}	54	8.5855e-02
2^{-23}	56	8.5855e-02
2^{-24}	58	8.5855e-02
2^{-25}	60	8.5855e-02
2^{-26}	62	8.5855e-02
2^{-27}	64	8.5855e-02
2^{-28}	66	8.5855e-02
2^{-29}	68	8.5855e-02
2^{-30}	70	8.5855e-02
2^{-40}	92	8.5852e-02

TABLE 1 Maximum pointwise errors for different values of ε for Example 1 with $M_x = 20$ (initially) and $M_t = 20$

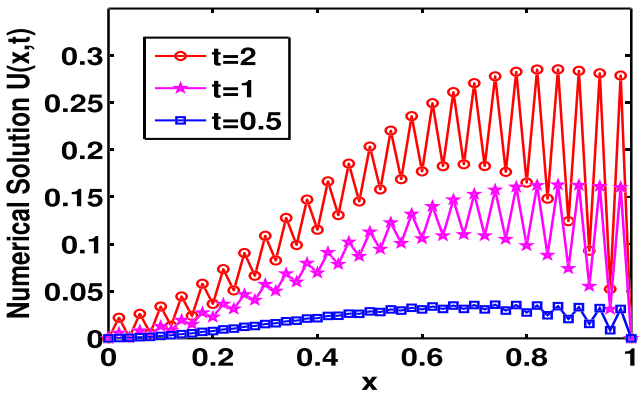

FIGURE 9 Oscillatory numerical solutions of Example 2 with $\varepsilon = 2^{-20}$, $M_x = 20$, and $M_t = 20$ on uniform mesh at different time levels [Colour figure can be viewed at wileyonlinelibrary.com]

There are several ways to use the one-dimensional approach to higher-dimensional problems. One of the popular techniques is alternating direction implicit method which uses the one-dimensional a priori meshes for solving two-dimensional time-dependent problems by decomposing it to two one-dimensional problems.

Example 2. Now, let us consider the following time-delayed SPPPDE[18]:

$$u_t - \varepsilon u_{xx} + (2 - x^2)u_x + (x + 1)(t + 1)u - u(x, t - 1) = 10t^2 \exp(-t)x(1 - x), \ \ (x, t) \in (0, 1) \times (0, 2],$$

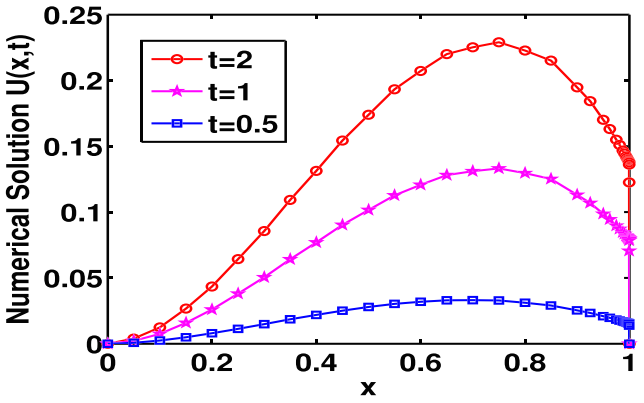

FIGURE 10 Nonoscillatory numerical solutions of Example 2 with $\varepsilon = 2^{-20}$, $M_x = 20$, $M_x^* = 50$, and $M_t = 20$ on adaptive mesh at different time levels [Colour figure can be viewed at wileyonlinelibrary.com]

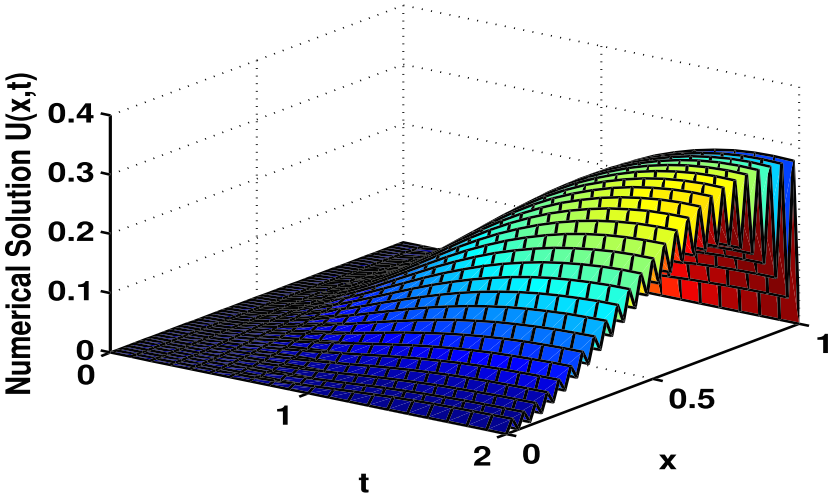

FIGURE 11 Oscillatory surface plot of Example 2 on uniform mesh for $\varepsilon = 2^{-20}$, $M_x = 20$, and $M_t = 20$ [Colour figure can be viewed at wileyonlinelibrary.com]

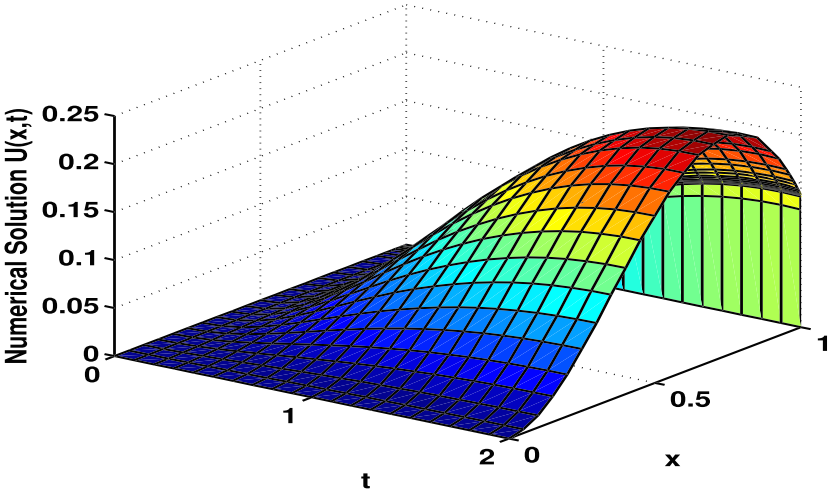

FIGURE 12 Nonoscillatory surface plot of Example 2 on the adaptive mesh for $\varepsilon = 2^{-20}$, $M_x = 20$, $M_x^* = 50$, and $M_t = 20$ [Colour figure can be viewed at wileyonlinelibrary.com]

with the initial data

$$u(x,t) = 0, \quad (x,t) \in [0,1] \times [-1,0],$$

and the boundary conditions

$$u(0,t) = 0, \ \textit{and} \ u(1,t) = 0, \quad t \in (0,2].$$

The numerical solution on uniform and spatial adaptive meshes are plotted in Figures 9 and 10, respectively, for Example 2 at different time levels. In addition, we also plot the surface solutions on these meshes at Figures 11 and 12 with $\varepsilon = 2^{-20}$ and $\wp = 1$. One can observe that the oscillatory behavior of the solution on a uniform mesh is removed by the generation of adaptive mesh. Adaptive spatial mesh generation for $\varepsilon = 2^{-20}$ with initial uniform mesh points 11 and 21 is presented at Figures 13 and 14. The maximum absolute errors are also presented in Table 2 for different values of ε.

Example 3. The following example is taken from Gowrisankar and Natesan[13] with a time delay:

$$u_t - \varepsilon u_{xx} + (2 - x^2)u_x + xu = u(x, t-1) + 10t^2 \exp(-t)x(1-x), \ (x,t) \in (0,1) \times (0,2],$$

with the initial data

$$u(x,t) = 0, \quad (x,t) \in [0,1] \times [-1,0],$$

and the boundary conditions

$$u(0,t) = 0, \ \textit{and} \ u(1,t) = 0, \quad t \in (0,2].$$

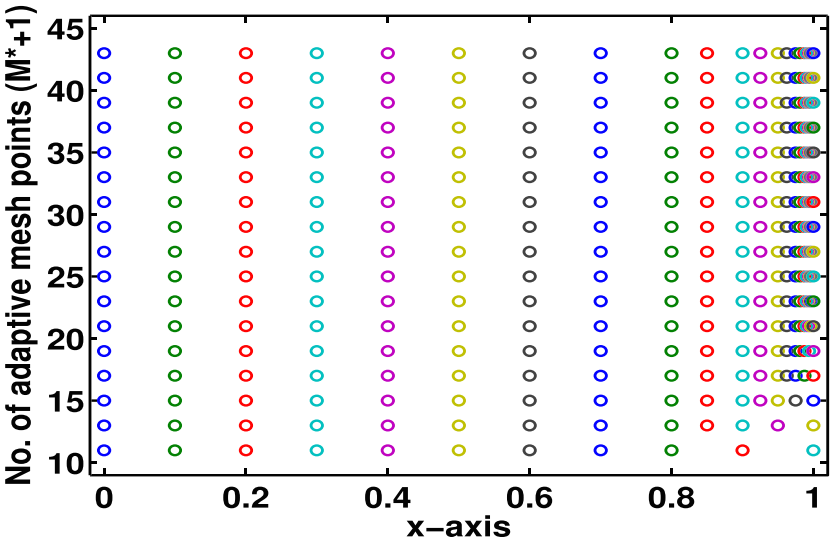

FIGURE 13 Generation of adaptive meshes from uniform meshes (starting with $M_x = 10$) for $\varepsilon = 2^{-20}$ at $t = 1/10$ for Example 2 [Colour figure can be viewed at wileyonlinelibrary.com]

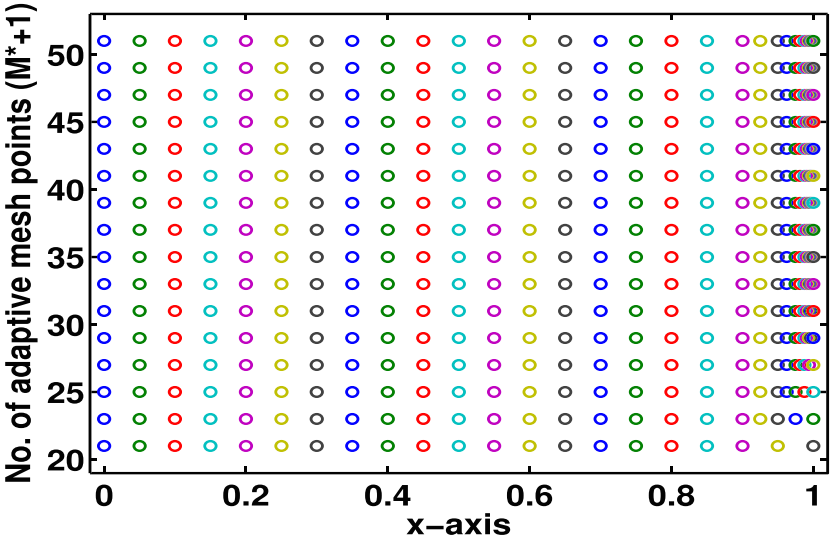

FIGURE 14 Generation of adaptive meshes from uniform meshes (starting with $M_x = 20$) for $\varepsilon = 2^{-20}$ at $t = 1/10$ for Example 2 [Colour figure can be viewed at wileyonlinelibrary.com]

To show the oscillatory and nonoscillatory behavior of the numerical solutions for Example 3, we have provided two Figures 15 and 16 on uniform and adaptive mesh, respectively, at different time levels for $\varepsilon = 2^{-30}$. Surface solution plots over all time levels are also provided on these meshes, at Figures 17 and 18. Adaptive mesh generation for $\varepsilon = 2^{-30}$ with initial uniform mesh points 11 and 21 is presented at Figures 19 and 20, which show that the adaptive mesh is dense towards the boundary layer region. In addition, the maximum absolute errors are also presented in Table 5 for few values of ε.

TABLE 2 Maximum pointwise errors for different values of ε for Example 2 with $M_x = 20$ (initially) and $M_t = 20$

ε	M_x^*	$E_\varepsilon^{M_x^*, M_t}$
2^{-10}	30	2.2039e-02
2^{-11}	32	2.2063e-02
2^{-12}	34	2.2076e-02
2^{-13}	36	2.2084e-02
2^{-14}	38	2.2087e-02
2^{-15}	40	2.2089e-02
2^{-16}	42	2.2090e-02
2^{-17}	44	2.2090e-02
2^{-18}	46	2.2090e-02
2^{-19}	48	2.2090e-02
2^{-20}	50	2.2090e-02
2^{-21}	52	2.2090e-02
2^{-22}	54	2.2090e-02
2^{-23}	56	2.2090e-02
2^{-24}	58	2.2090e-02
2^{-25}	60	2.2090e-02
2^{-26}	62	2.2090e-02
2^{-27}	64	2.2090e-02
2^{-28}	66	2.2090e-02
2^{-29}	68	2.2090e-02
2^{-30}	70	2.2090e-02
2^{-40}	92	2.2090e-02

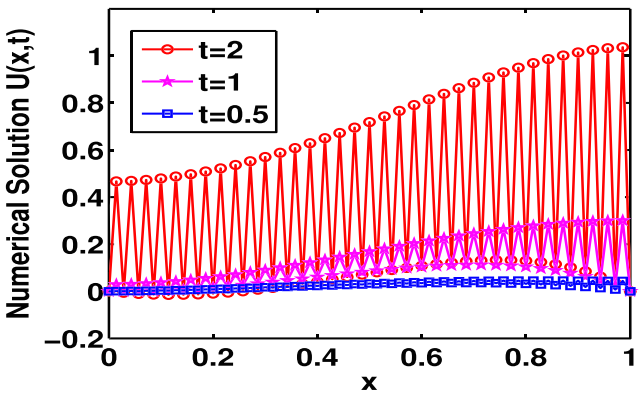

FIGURE 15 Oscillatory numerical solutions of Example 3 on uniform mesh with $\varepsilon = 2^{-30}$, $M_x = 20$ and $M_t = 20$ at different time levels [Colour figure can be viewed at wileyonlinelibrary.com]

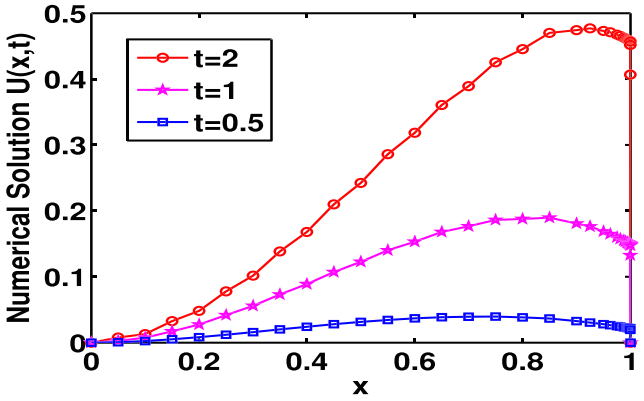

FIGURE 16 Numerical solutions of Example 3 on adaptive mesh with $\varepsilon = 2^{-30}$, $M_x = 20$, $M_x^* = 70$, and $M_t = 20$ at different time levels [Colour figure can be viewed at wileyonlinelibrary.com]

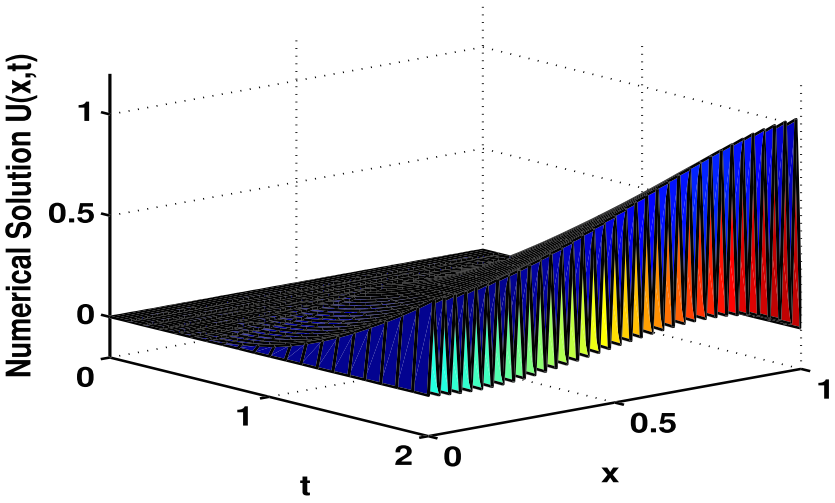

FIGURE 17 Oscillatory solution surface plot of Example 3 on uniform mesh for $\epsilon = 2^{-30}$, $M_x = 20$, $M_x^* = 70$, and $M_t = 20$ [Colour figure can be viewed at wileyonlinelibrary.com]

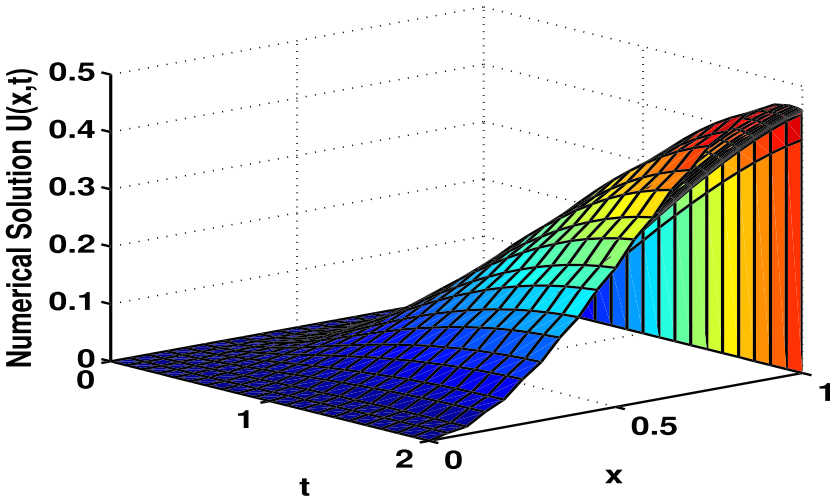

FIGURE 18 Nonoscillatory solution surface plot of Example 3 on adaptive mesh for $\epsilon = 2^{-30}$, $M_x = 20$, $M_x^* = 70$, and $M_t = 20$ [Colour figure can be viewed at wileyonlinelibrary.com]

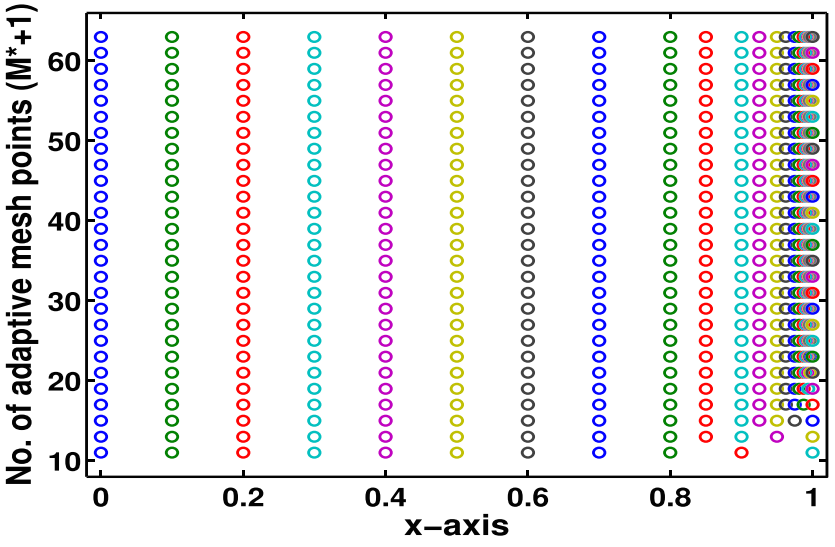

FIGURE 19 Generation of adaptive meshes from uniform meshes (starting with $M_x = 10$) for $\epsilon = 2^{-30}$ at $t = 1/10$ for Example 3 [Colour figure can be viewed at wileyonlinelibrary.com]

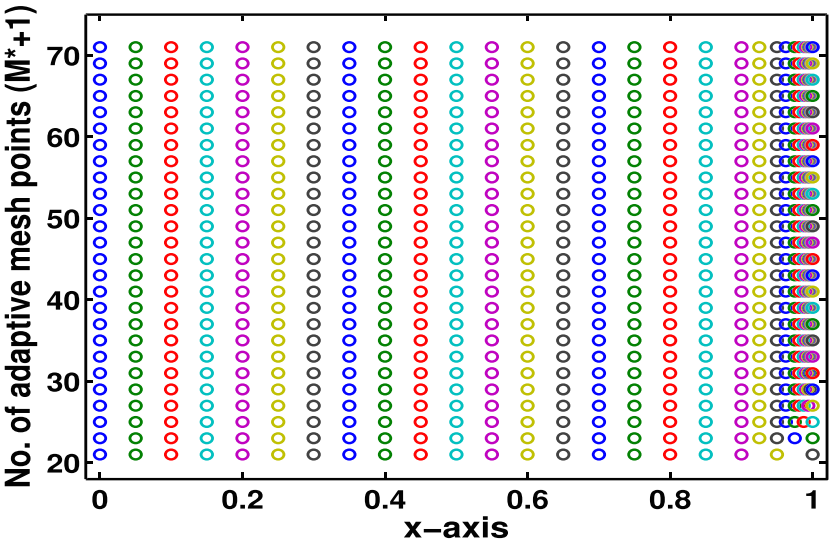

FIGURE 20 Generation of adaptive meshes from uniform meshes (starting with $M_x = 20$) for $\varepsilon = 2^{-30}$ at $t = 1/10$ for Example 3 [Colour figure can be viewed at wileyonlinelibrary.com]

TABLE 3 Maximum pointwise errors for different values of ε for Example 3 with $M_x = 20$ (initially) and $M_t = 20$

ε	M_x^*	$E_\varepsilon^{M_x^*,M_t}$
2^{-10}	30	5.3985e-02
2^{-11}	32	5.4354e-02
2^{-12}	34	5.4611e-02
2^{-13}	36	5.4746e-02
2^{-14}	38	5.4817e-02
2^{-15}	40	5.4855e-02
2^{-16}	42	5.4879e-02
2^{-17}	44	5.4891e-02
2^{-18}	46	5.4897e-02
2^{-19}	48	5.4900e-02
2^{-20}	50	5.4902e-02
2^{-21}	52	5.4903e-02
2^{-22}	54	5.4903e-02
2^{-23}	56	5.4903e-02
2^{-24}	58	5.4903e-02
2^{-25}	60	5.4903e-02
2^{-26}	62	5.4903e-02
2^{-27}	64	5.4903e-02
2^{-28}	66	5.4903e-02
2^{-29}	68	5.4903e-02
2^{-30}	70	5.4903e-02
2^{-40}	92	5.4902e-02

Table 3 provides the maximum point-wise error for the Example 3 based on the presently proposed graded mesh. Table 4 uses the equidistributed mesh[37] to solve the time-delayed model in Example 3. This shows that the equidistributed mesh explained in previous works[11,27,28,37,41] is more effective compared to present graded mesh for boundary layer adaptive solutions as one observes less errors on equidistributed mesh.

Example 4. We consider the following singularly perturbed time delay problem:

$$u_t - \varepsilon u_{xx} + xtu_x + (x+1)(t+1)u = u(x, t-1) + 10t^2 \exp(-t)x(1-x), \ (x,t) \in (0,1) \times (0,2],$$

with the initial data

$$u(x,t) = 0, \quad (x,t) \in [0,1] \times [-1,0],$$

and the boundary conditions

$$u(0,t) = 0, \ \textit{and} \ u(1,t) = 0, \quad t \in (0,2].$$

TABLE 4 Maximum pointwise errors by equidistributed mesh for different values of ε for Example 3 with $M_x = 20$ and $M_t = 20$

ε	M_x	$E_\varepsilon^{M_x,M_t}$
2^{-11}	20	0.0484
2^{-12}	20	0.0489
2^{-13}	20	0.0492
2^{-14}	20	0.0493
2^{-15}	20	0.0452
2^{-16}	20	0.0453
2^{-17}	20	0.0464
2^{-18}	20	0.0470
2^{-19}	20	0.0471
2^{-20}	20	0.0471
2^{-21}	20	0.0479
2^{-22}	20	0.0480
2^{-23}	20	0.0487
2^{-24}	20	0.0496
2^{-25}	20	0.0488
2^{-26}	20	0.0517
2^{-27}	20	0.0496
2^{-28}	20	0.0509
2^{-29}	20	0.0536
2^{-30}	20	0.0537

TABLE 5 Maximum pointwise errors for different values of ε for Example 4 with $M_x = 20$ (initially) and $M_t = 20$

ε	M_x^*	$E_\varepsilon^{M_x^*,M_t}$
2^{-10}	32	5.0014e-02
2^{-11}	34	5.0100e-02
2^{-12}	36	5.0141e-02
2^{-13}	38	5.0159e-02
2^{-14}	40	5.0168e-02
2^{-15}	42	5.0172e-02
2^{-16}	44	5.0174e-02
2^{-17}	46	5.0175e-02
2^{-18}	48	5.0175e-02
2^{-19}	50	5.0175e-02
2^{-20}	52	5.0176e-02
2^{-21}	54	5.0176e-02
2^{-22}	56	5.0176e-02
2^{-23}	58	5.0176e-02
2^{-24}	60	5.0176e-02
2^{-25}	62	5.0176e-02
2^{-26}	64	5.0176e-02
2^{-27}	66	5.0176e-02
2^{-28}	68	5.0176e-02
2^{-29}	70	5.0176e-02
2^{-30}	72	5.0176e-02
2^{-40}	94	5.0176e-02

The maximum absolute errors are presented in Table 5 for Example 4 for different values of ε.

6 | CONCLUSIONS

In this article, we have proposed an adaptive mesh refinement algorithm to solve a class of time-delayed SPPPDE. Due to the use of highly accurate central difference scheme for discretization, numerical solution produces nonphysical oscillations. Our present algorithm adaptively introduces new mesh points based on an entropy function inside the oscillatory regions. The present approach produces oscillation-free boundary layer adaptive solution by starting with a small number of uniform mesh points. Numerical experiments show that the present algorithm is very effective for boundary layer approximation.

ACKNOWLEDGEMENTS

The authors are thankful to the referees for bringing the required improvements for the present manuscript. The author, Pratibhamoy Das, wants to thank the Science and Engineering Research Board (SERB), Govt. of India, for providing the research support for the present work under the grant ECR/2017/001973.

CONFLICT OF INTEREST

This work does not have any conflicts of interest.

ORCID

Kamalesh Kumar https://orcid.org/0000-0002-2527-3836
Pramod Chakravarthy Podila https://orcid.org/0000-0002-5540-6302
Pratibhamoy Das https://orcid.org/0000-0001-5095-0360
Higinio Ramos https://orcid.org/0000-0003-2791-6230

REFERENCES

1. Musila M, Lansky P. Generalized Stein's model for anatomically complex neurons. *BioSystems*. 1991;25(3):179-191.
2. Arino O, Hbid ML, Dads EA. *Delay Differential Equations and Applications*. Berlin: Springer; 2006.
3. Murray JD. *Mathematical Biology I: An Introduction*. 3rd ed. Berlin: Springer-Verlag; 2001.
4. Cheng O, Jia-qi M. The nonlinear singularly perturbed problems for predator-prey reaction diffusion equation. *J Biomath*. 2005;20(2):135-141.
5. Wu J. *Theory and Applications of Partial Functional Differential Equations*. New York: Springer; 1996.
6. Lange CG, Miura RM. Singular perturbation analysis of boundary-value problems for differential-difference equations. *SIAM J Appl Math*. 1982;42:502-531.
7. Rao RN, Chakravarthy PP. A fitted numerov method for singularly perturbed parabolic partial differential equations with a small negative shift arising in control theory. *Numer Math Theor Meth Appl*. 2014;7(1):23-40.
8. Kadalbajoo MK, Sharma KK. Numerical analysis of singularly perturbed delay differential equations with layer behavior. *J Comput Appl Math*. 2004;157:11-28.
9. Kadalbajoo MK, Sharma KK. Parameter-Uniform fitted mesh method for singularly perturbed delay differential equations with layer behavior. *Electron Trans Numer Anal*. 2006;23:180-201.
10. Kadalbajoo MK, Sharma KK. A numerical method based on finite difference for boundary value problems for singularly perturbed delay differential equations. *Appl Math Comput*. 2008;197:692-707.
11. Das P. An a posteriori based convergence analysis for a nonlinear singularly perturbed system of delay differential equations on an adaptive mesh. *Numer Algorithms*. 2019;81:465-487.
12. Ansari AR, Bakr SA, Shishkin GI. A parameter-robust finite difference method for singularly perturbed delay parabolic partial differential equations. *J Comput Appl Math*. 2007;205:552-566.
13. Gowrisankar S, Natesan S. ε- uniformly convergent numerical scheme for singularly perturbed delay parabolic partial differential equations. *Int J Comput Math*. 2017;94(5):902-921.
14. Das P, Rana S, Ramos H. On the approximate solutions of a class of fractional order nonlinear Volterra integro-differential initial value problems and boundary value problems of first kind and their convergence analysis. *J Comput and Appl Math*. 2020:113116. https://doi.org/10.1016/j.cam.2020.113116
15. Das P, Rana S, Ramos H. Homotopy perturbation method for solving Caputo type fractional order Volterra-Fredholm integro-differential equations. *Comput Math Methods*. 2019. https://doi.org/10.1002/cmm4.1047
16. Das P, Rana S, Ramos H. A perturbation based approach for solving fractional order Volterra-Fredholm integro differential equations and its convergence analysis. *Int J Comput Math*. 2020;97(10):1994-2014.
17. Santra S, Mohapatra J. Analysis of the L1 scheme for a time fractional parabolic–elliptic problem involving weak singularity. *Math Methods Appl Sci*. 2020. https://doi.org/10.1002/mma.6850
18. Das A, Natesan S. Second-order uniformly convergent numerical method for singularly perturbed delay parabolic partial differential equations. *Int J Comput Math*. 2018;95(3):490-510.
19. Chandru M, Das P, Ramos H. Numerical treatment of two-parameter singularly perturbed parabolic convection diffusion problems with non-smooth data. *Math Methods Appl Sci*. 2018;41:5359-5387.
20. Chandru M, Prabha T, Das P, Shanthi V. A numerical method for solving boundary and interior layers dominated parabolic problems with discontinuous convection coefficient and source terms. *Differ Equ Dyn Syst*. 2019;27:91-112.
21. L Govindarao J, Mohapatra A. Das a fourth-order numerical scheme for singularly perturbed delay parabolic problem arising in population dynamics. *J Appl Math Computing*. 2020;63:171-195.

22. Bansal K, Sharma KK. Parameter uniform numerical scheme for time dependent singularly perturbed convection-diffusion-reaction problems with general shift arguments. *Numer Algorithms*. 2017;75(1):113-145.
23. Bansal K, Rai P, Sharma KK. Numerical treatment for the class of time dependent singularly perturbed parabolic problems with general shift arguments. *Differ Equ Dyn Syst*. 2017;25(2):327-346.
24. Chakravarthy PP, Kumar K. An adaptive mesh method for time dependent singularly perturbed differential-difference equations. *Nonlinear Eng*. 2019;8(1):328-339.
25. Das P. Comparison of a priori and a posteriori meshes for singularly perturbed nonlinear parameterized problems. *J Comput Appl Math*. 2015;290:16-25.
26. Das P. A higher order difference method for singularly perturbed parabolic partial differential equations. *J Difference Equations and Applications*. 2018;24(3):452-477.
27. Das P, Rana S, Vigo-Aguiar J. Higher order accurate approximations on equidistributed meshes for boundary layer originated mixed type reaction diffusion systems with multiple scale nature. *Appl Numer Math*. 2020;148:79-97.
28. Shakti D, Mohapatra J, Das P, Vigo-Aguiar J. A moving mesh refinement based optimal accurate uniformly convergent computational method for a parabolic system of boundary layer originated reaction diffusion problems with arbitrary small diffusion terms. *J Comput Appl Math*. 2020. https://doi.org/10.1016/j.cam.2020.113167
29. Shakti D, Mohapatra J. Numerical simulation and convergence analysis for a system of nonlinear singularly perturbed differential equations arising in population dynamics. *J Difference Equations and Appl*. 2018;24(7):1185-1196.
30. Das P, Natesan S. Numerical solution of a system of singularly perturbed convection-diffusion boundary-value problems using mesh equidistribution technique. *Aust J Math Anal Appl*. 2013;10(1):1-17.
31. Bakhvalov NS. On the optimization of the methods for solving boundary value problems in the presence of boundary layers. *Zh Vychisl Mater Fiz*. 1969;9:841-859.
32. Gartland EC. Graded-mesh difference schemes for singularly perturbed two-point boundary value problems. *Math Comput*. 1988;51(184):631-657.
33. Beckett MG, Mackenzie JA. Convergence analysis of finite difference approximations on equidistribted grids to a singularly perturbed boundary value problem. *Appl Numer Math*. 2000;35:87-109.
34. Beckett MG, Mackenzie JA. On a uniformly accurate finite difference approximation of a singularly perturbed reaction diffusion problem using grid equidistribution. *J Comput Appl Math*. 2001;131:381-405.
35. Kumar V, Srinivasan B. An adaptive mesh strategy for singularly perturbed convection diffusion problems. *Appl Math Model*. 2015;39:2081-2091.
36. Solonnikov VA, Ladyzenskaja OA, Ural'ceva NN. *Linear and Quasi Linear Equations of Parabolic Type*. Rhode Island: American Mathematical Society Providence; 1988.
37. Das P, Mehrmann V. Numerical solution of singularly perturbed parabolic convection-diffusion- reaction problems with two small parameters. *BIT Numerical Math*. 2016;56:51-76.
38. Andreev VB, Kopteva N. On the convergence, uniform with respect to a small parameter, of monotone three point finite difference approximations. *Differential Equa*. 1998;34(7):921-928.
39. Leveque R. *Finite Volume Methods For Hyperbolic Problems*. Cambridge University Press; 2002.
40. Doolan EP, Miller JJH, Schilders WHA. *Uniform Numerical Methods for Problems with Initial and Boundary Layers*. Dublin: Boole Press; 1980.
41. Das P, Vigo-Aguiar J. Parameter uniform optimal order numerical approximation of a class of singularly perturbed system of reaction diffusion problems involving a small perturbation parameter. *J Comput Appl Math*. 2019;24(3):533-544.

How to cite this article: Kumar K, Podila PC, Das P, Ramos H. A graded mesh refinement approach for boundary layer originated singularly perturbed time-delayed parabolic convection diffusion problems. *Math Meth Appl Sci*. 2021;44:12332–12350. https://doi.org/10.1002/mma.7358